Journal of Magnetic Resonance 210 (2011) 133–136

Contents lists available at ScienceDirect

Journal of Magnetic Resonance

journal homepage: www.elsevier.com/locate/jmr

Communication

Single-slice mapping of ultrashort T_2

Stefan Kirsch *, Lothar R. Schad

Computer Assisted Clinical Medicine, Heidelberg University, Mannheim, Germany

ARTICLE INFO

Article history:
Received 10 November 2010
Revised 1 February 2011
Available online 26 February 2011

Keywords:
Transverse relaxation
Ultrashort echo time (UTE) magnetic resonance imaging
Short T_2
Muscoloskeletal tissue
Bone
Cartilage
Tendon
Sodium-23
Chlorine-35
Oxygen-17

ABSTRACT

In this communication we present a method for single-slice mapping of ultrashort transverse relaxation times T_2. The RF pulse sequence consists of a spin echo preparation of the magnetization followed by slice-selective ultrashort echo time (UTE) imaging with radial *k*-space sampling. In order to keep the minimum echo time as small as possible, avoid out-of-slice contamination and signal contamination due to unwanted echoes, the implemented pulse sequence employs a slice-selective 180° RF refocusing pulse and a 4-step phase cycle. The slice overlap of the two slice-selective RF pulses was investigated. An acceptable Gaussian slice profile could be achieved by adjusting the strength of the two slice-selection gradients. The method was tested on a short T_2 phantom consisting of an arrangement of a roll of adhesive tape, an eraser, a piece of modeling dough made of Plasticine®, and a 10% w/w agar gel. The T_2 measurements on the phantom revealed exponential signal decays for all samples with T_2(adhesive tape) = (0.5 ± 0.1) ms, T_2(eraser) = (2.33 ± 0.07) ms, T_2(Plasticine®) = (2.8 ± 0.06) ms, and T_2(10% agar) = (9.5 ± 0.83) ms. The T_2 values obtained by the mapping method show good agreement with the T_2 values obtained by a non-selective T_2 measurement. For all samples, except the adhesive tape, the effective transverse relaxation time T_2^* was significantly shorter than T_2. Depending on the scanner hardware the presented method allows mapping of T_2 down to a few hundreds of microseconds. Besides investigating material samples, the presented method can be used to study the rapidly decaying MR-signal from biological tissue (e.g.: bone, cartilage, and tendon) and quadrupolar nuclei (e.g.: ^{23}Na, ^{35}Cl, and ^{17}O).

1. Introduction

Measurement of the transverse relaxation time T_2 is one of the most established techniques to characterize material samples or biological tissue by means of NMR. The value of T_2 is directly connected to the molecular mobility of the spin bearing molecules under investigation. Molecular motion in context with NMR is classified into different regimes. High molecular mobility as typically occurring in liquid-like samples is characterized by short molecular correlation times τ_c (tens of picoseconds). In the so-called "extreme narrowing" regime ($\tau_c \ll \omega_0^{-1}$, ω_0 = Larmor frequency) the Bloembergen-Purcell-Pound theory (BPP-theory) is used to quantitatively describe relaxation times of spin 1/2 nuclei [1]. Within this regime the decay of the transverse magnetization shows exponential behavior and the values of the relaxation times are typically in the range of several tens or hundreds of milliseconds. If the mobility of the spin bearing molecules is restricted so that averaging of direct dipole–dipole interactions becomes less effective, extremely short T_2 values are expected and the BPP-theory may no longer be valid. As a result of the non-averaged dipole–dipole interactions, non-exponential signal decays may be observed which can be handled by alternative theoretical approaches (e.g. the Anderson–Weiss approach [2]). This situation is partially given for short T_2 biological tissues like cortical bone, cartilage or tendon where T_2 values of a few milliseconds or less are observed [3,4]. Extremely short T_2 values are also reported for protons in lung tissue [5], ^{31}P in bone minerals [6,7], and quadrupolar nuclei like ^{23}Na, ^{35}Cl, and ^{17}O [8–10]. In this communication we present a slice-selective MRI method for mapping of ultrashort T_2. The method utilizes fast T_2 preparation of the magnetization by a spin echo followed by ultrashort echo time (UTE) imaging. Depending on the scanner hardware, the presented method allows mapping of T_2 values down to a few hundreds of microseconds.

2. Methods

2.1. Hardware and phantom setup

All the experiments were performed on a 9.4 T Bruker Biospec 94/20 USR small animal system equipped with 740 mT/m *x*, *y*, *z*-gradients. The experiments were performed with a ^{1}H quadrature volume transmit/receive resonator of 7.2 cm in diameter.

The phantoms consist of an arrangement of a roll of adhesive tape (Tesa®, Germany), an eraser (Laeufer® SW-0240, Germany),

* Corresponding author. Address: Computer Assisted Clinical Medicine, Heidelberg University, Theodor-Kutzer-Ufer 1-3, D-68167 Mannheim, Germany. Fax: +49 621 383 5123.
E-mail address: stefan.kirsch@medma.uni-heidelberg.de (S. Kirsch).

1090-7807/$ - see front matter © 2011 Elsevier Inc. All rights reserved.
doi:10.1016/j.jmr.2011.02.003

modeling dough made of Plasticine® (GLOREX, Switzerland) and a 4% or 10% w/w agar gel.

2.2. RF pulse sequences

The RF pulse sequence used for the T_2 measurements (Fig. 1a) can be divided into two parts: (i) a T_2 preparation interval and (ii) a slice-selective UTE [11] image readout with radial k-space sampling. During the T_2 preparation interval the magnetization is prepared according to a spin echo with variable echo time TE. The transverse magnetization at $t = TE$ is stored longitudinally by the second 90° RF pulse. The use of this preparation scheme ensures shortest minimum TE. After dephasing of residual transverse magnetization by spoiler gradients, the image is acquired by a slice-selective Gaussian half-pulse with succeeding radial k-space sampling. In contrast to the method presented recently by Du et al. [14], the RF pulses are applied using a 4-step phase cycle and the 180° RF refocusing pulse is applied in presence of a slice-selection gradient. The implemented phase cycle reads: ϕ = const. = x, $\varphi = (y, y, -y, -y)$, $\theta = (-x, x, -x, x)$, υ = const. = x, and receiver phase = $(-x, x, -x, x)$. The phase-cycling scheme and the use of a slice-selective refocusing RF pulse were motivated by the following considerations:

1. Immediately *after* the second 90° RF pulse (“flip-back pulse”) residual magnetization can remain in the longitudinal direction which does not originate from the spin echo. This residual magnetization can result from imperfections in the flip angles of the previous RF pulses and it can contaminate the useful signal. The constant phase υ of the slice-selective 90° RF pulse and the alternation of the receiver phase prevent signal contamination owing to this residual longitudinal magnetization.
2. Imperfections in the flip angle of the 180° refocusing RF pulse can generate unwanted transverse magnetization. In order to avoid contamination of the echo signal at $t = TE$ with this kind of magnetization, the phase φ of the 180° RF pulse is switched by 180° every two steps.
3. In addition to point 2, imperfections in the flip angle of the 180° RF pulse can generate a stimulated echo (STE) at $t = (3/2)\cdot TE + t_{sp}$. The phase of this STE is given by $\upsilon + \theta - \varphi + 180°$ [15]. From the implemented phase cycle follows: phase (STE) = $\theta - \varphi$ + const., thus the phase of the STE will alternate by 180°. The likewise 180° alternation of the receiver phase is not able to filter out the STE. However, the 180° RF pulse is applied in presence of the magnetic field gradient G_{s1}. Since the gradient G_{s1} is not balanced during the image readout, it prevents formation of the STE. The gradient strength G_{s1} was chosen according to

$$G_{s1} = G_{s2}\frac{BW_{180}}{c \cdot BW_{90}} \tag{1}$$

Here, BW_{180} = bandwidth of the 180° RF pulse, BW_{90} = bandwidth of the 90° Gaussian half-pulse and $c = d_{180}/d_{90}$ is the ratio of the apparent slice thicknesses d_{90} (image readout) and d_{180} (180° refocusing RF pulse). The gradient strength G_{s2} was calculated by the scanner software according to $G_{s2} = 2\pi\cdot BW_{90}/(\gamma\cdot d_{90})$, where γ = gyromagnetic ratio. The idea behind Eq. (1) is to set the ratio c such that the resulting slice overlap (180° block-pulse → sinc slice profile, 90° Gaussian half-pulse → Gaussian slice profile) resembles an acceptable Gaussian slice profile which is smooth and almost free of side lobes.

Optimization of the ratio c was done using the RF pulse sequence shown in Fig. 1b. The magnetization is first inverted by a slice-selective 180° RF block-pulse. After dephasing of residual transverse magnetization a second slice-selective 90° RF Gaussian half-pulse is applied. In the next step, the transverse magnetization resulting from the two slice selections is dephased by spoiler gradients. The following slice-selective imaging procedure is applied on an orthogonal gradient direction, thus the slice profile resulting from the slice overlap should be visible as dark area in the image. For the optimization measurements the following parameters were used: TR = 70 ms, t_d = 44 μs, d_{90} = 2 mm, number of projections = 268, field of view (FOV) = (64×64) mm^2, matrix = 128 × 128, number of dummy scans = 16, bandwidth (BW) = 1.9 kHz/pix-

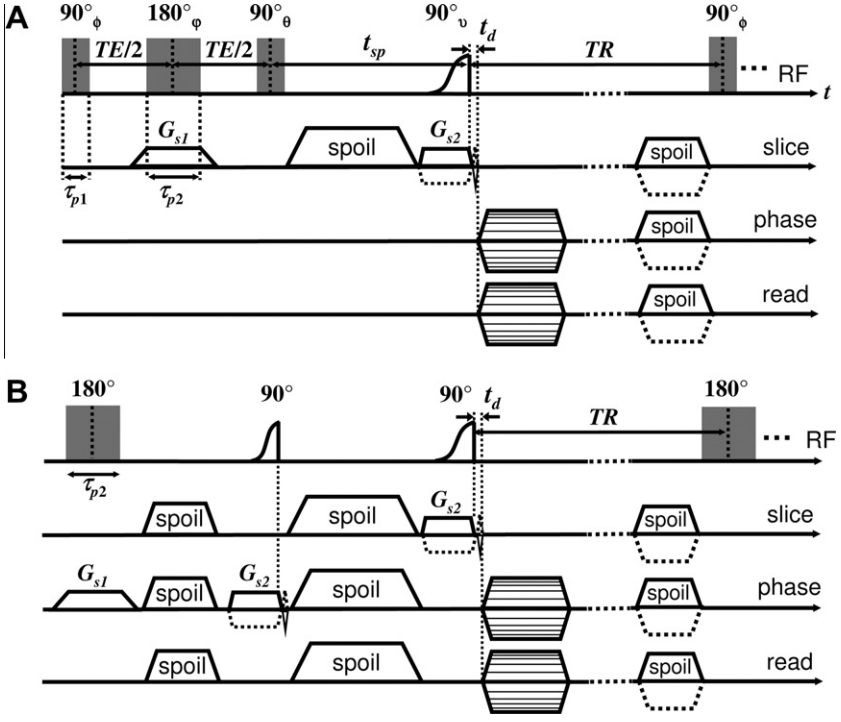

Fig. 1. (a) RF pulse sequence used for the T_2 mapping. (b) RF pulse sequence used for the optimization of the slice profile.

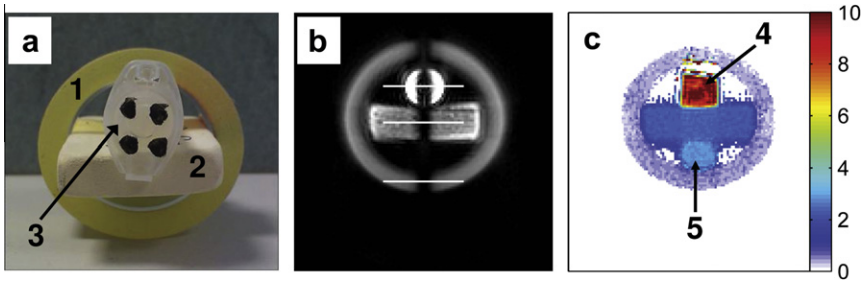

Fig. 2. (a) Picture of the phantom used for the slice profile measurement. 1 = adhesive tape, 2 = eraser and 3 = 4% w/w agar gel. (b) MR image resulting from the slice profile optimization experiment (RF pulse sequence shown in Fig. 1b). The white bars indicate the lines which were used for the analysis of the slice profiles. (c) T_2 mapping. 4 = 10% agar gel, 5 = piece of Plasticine®. The T_2 values are given in ms.

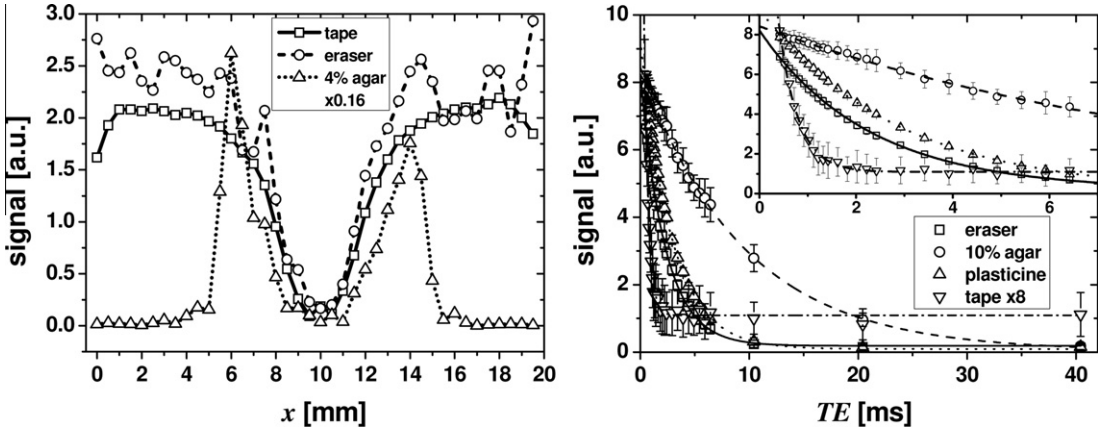

Fig. 3. (Left) slice profiles taken from the lines indicated in Fig. 2b. (Right) signal decays and curve fits taken from an exemplary ROI within the different samples.

el, and scan time = 1 min 28 s. An optimal value of $c = 1.5$ was found and used for the T_2 mapping.

2.3. T_2 mapping

A map of the transverse relaxation time T_2 was measured by incrementing the echo time TE in the range of 0.42 up to 40.42 ms with 27 increments. The parameters for the T_2 measurement were: $TR = 70$ ms, $t_d = 44$ μs, $d_{90} = 2$ mm, number of projections = 268, FOV = (64×64) mm^2, matrix = 128×128, $BW = 1.9$ kHz/pixel, number of dummy scans = 16, $\tau_{p1} = \tau_{p2}/2 = 40$ μs, and scan time = 2 min 56 s (for $TE = 0.42$ ms). Note, the scan time increases with increasing TE. The scan time for $TE = 40.42$ ms was 4 min 27 s. The total measurement time for all 27 increments was approximately 1 h 20 min. The measured signal intensity S_i of the ith pixel was fitted to

$$S_i(TE) = S_{0,i} \cdot \exp(-TE/T_{2,i}) + y_{0,i} \quad (2)$$

Here, $S_{0,i}$ = scaling constant, $T_{2,i}$ = value of the transverse relaxation time and $y_{0,i}$ is the offset of the ith pixel. Note, that we assume for simplicity an exponential decay of the magnetization which generally may not be justified, in particular in samples with restricted molecular mobility. The simplification was motivated by our experimental results and it will be discussed in detail in the discussion section of this communication. The curve fitting procedures for the T_2 mapping were performed using Matlab® (Mathworks, USA).

2.4. Non-localized measurement of T_2 and T_2^*

In order to verify the results of the T_2 mapping, a non-selective spin echo sequence of the type $[(90)_{\sigma 1} - TE/2 - (180)_{\sigma 2} - TE/2 - (\mathrm{ACQ})_{\sigma 3} - \pm G_{sp}]_{TR}$ was implemented. Here, ACQ = data acquisition, $\pm G_{sp}$ = alternated spoiler gradient in x,y,z direction, TR = repetition time = 1 s, σx = RF pulse and receiver phase cycle with $\sigma 1 = (x, x, -x, -x)$, $\sigma 2 = (y, -y, y, -y)$, and $\sigma 3 = (x, x, -x, -x)$. The durations of the RF pulses, the number of TE increments, and the TE timing were the same as in the T_2 mapping measurement. The data processing for the determination of T_2 was as follows: calculation of the on-resonance magnitude mode $\mathrm{FID}(t_{ACQ},TE) \rightarrow$ integration over $t_{ACQ} \rightarrow I(TE) = S(TE) \rightarrow$ fit to Eq. (2). Processing for determination of T_2^*: calculation of the on-resonance magnitude mode $\mathrm{FID}(t_{ACQ}) = S(t_{ACQ}) \rightarrow$ fit to Eq. (2) with $TE \rightarrow t_{ACQ}$ and $T_2 \rightarrow T_2^*$.

3. Results

The slice profile measurement was performed on an arrangement of the adhesive tape, the 4% agar gel, and the easer (see Fig. 2a). The slice profiles were measured with the ratio $c = 1.5$. A setting of $d_{90} = 2$ mm resulted in an acceptable total Gaussian slice profile with a half-height-width of approximately 4 mm (see Figs. 2b and 3).

T_2 mapping was done on an arrangement of the adhesive tape, the 10% agar gel, the eraser and a piece of Plasticine®. Note that the 10% agar gel was used *without* a container. Fig. 2c shows the T_2 map obtained by the pixel-wise curve fitting procedure. Exemplary signal decays from selected ROIs within the different samples are shown in Fig. 3 and the corresponding T_2 values are given in Table 1.

The results of the non-selective T_2 and T_2^* measurements are given in Table 1. The measured background signal originating from the sample holder and the coil encasement was two magnitudes smaller than the signal of the adhesive tape. Therefore, the background signal was neglected in the fitting procedures. For all sam-

Table 1
Results of the T_2 mapping and the non-selective T_2/T_2^* measurement.

	10% agar	Eraser	Plasticine®	Adhesive tape
T_2 (map) (ms)	9.5 ± 0.83	2.33 ± 0.07	2.8 ± 0.06	0.5 ± 0.1
Number of pixels in ROI	74	152	46	28
T_2 (non-sel. meas.) (ms)	7.6 ± 0.78	2.35 ± 0.2	2.89 ± 0.61	0.47 ± 0.1
T_2^* (ms)	1.15 ± 0.02	0.31 ± 0.01	0.37 ± 0.01	0.27 ± 0.01

ples, except the adhesive tape, the effective transverse relaxation time T_2^* was significantly shorter than T_2.

4. Discussion

The use of a short *TR* generates a small steady-state magnetization and hence a low signal-to-noise ratio (SNR). If necessary, the SNR can be improved by increasing *TR* values, which in turn leads to an increase of the total measurement time. The choice of *TR* depends on finding a compromise between the desired accuracy of the measured T_2 values and the available measurement time. In our experiments a value of $TR = 70$ ms and a 4-step phase cycle was sufficient to get a reasonable SNR.

The minimum *TE* value depends on the durations of the first three RF pulses and on the ramp time of the slice-selection gradient G_{s1}. The minimum *TE* value may vary for different scanners, because these time delays depend on the filling factor of the coil, the maximum transmitter power, and the gradient slew rate. In order to optimize the minimum *TE*, we used a block-shaped 180° refocusing pulse. A block-shaped RF pulse has the best RF power efficiency (flip angle/duration). However, a major drawback of the block-shaped RF pulse is its slice profile. The side lobes of the sinc profile impede sharp slice selection. Nevertheless, the influence of the side lobes can be minimized to a tolerable degree by optimizing the ratio *c*. The measured slice profile for $c = 1.5$ shows an acceptable Gaussian profile almost free of side lobes (Fig. 3). A value of $d_{90} = 2$ mm resulted in an acceptable total Gaussian slice profile with a half-height-width of approximately 4 mm. In experiments where only a certain region of the sample is of interest and the total measurement time is the limiting factor, a single-slice imaging method could be beneficial, because 2D *k*-space sampling is less time-consuming than 3D *k*-space sampling (e.g. as used in Refs. [12,13]).

The T_2 values obtained by the mapping method were in good agreement with the T_2 values measured by the non-selective method. However, there was a slight difference in the T_2 value of the 10% agar gel which may be related to radiation damping [16,17]. It is well known, that radiation damping is able to interfere the determination of relaxation times (shorter apparent T_1 and T_2). The strength of this shortening effect increases with increasing magnitude of the transverse magnetization during the spin echo preparation [16,17]. Since highest signal intensity was observed in the non-selective T_2 measurement of the 10% agar gel, the shortening effect is expected to be most pronounced in this measurement. The slightly shorter T_2 value of the 10% agar gel measured by the non-selective method (7.6 *vs.* 9.5 ms) supports this speculation.

In the T_2 measurements we observed exponential signal decays for all samples. For the eraser, the piece of Plasticine® and the adhesive tape this observation may be unexpected, since signal decays resembling a superposition of a Gaussian and an exponential decay were proposed for samples consisting of cross-linked polymers [12]. In Ref. [12] T_2 relaxation times of rubber samples were measured using a 3D spin-echo back-projection sequence. The measured signal decays showed the proposed superposition of a Gaussian-like and an exponential function. The mismatch with our data may be related to the relatively long RF pulse durations used in our study ($\tau_{p1} = \tau_{p2}/2 = 40$ μs *vs.* $\tau_{p1} = 1.5$ μs in Ref. [12]). As a consequence of long $\tau_{p1,2}$ the minimum possible echo time was 420 μs. During this time the Gaussian signal contribution, which is associated with the slowly moving inter-cross-link chains of the polymer network [12], is almost fully relaxed, and therefore only the exponential part of the signal decay is observable.

The presented method could be useful in ^{1}H T_2 mapping of material samples or biological tissues with ultrashort T_2 like tendon, cartilage, and bone. Despite the measurements provided in this communication are performed solely on the ^{1}H nucleus, the method could also be practicable to other nuclei, e.g. ^{23}Na, ^{35}Cl and ^{17}O.

References

[1] N. Bloembergen, E. Purcell, R. Pound, Relaxation effects in nuclear magnetic resonance absorption, Phys. Rev. 73 (1948) 679–746.
[2] P.W. Anderson, P.R. Weiss, Exchange narrowing in paramagnetic resonance, Rev. Mod. Phys. 25 (1953) 269–276.
[3] R.M. Henkelman, G.J. Stanisz, J.K. Kim, M.J. Bronskill, Anisotropy of NMR propreties of tissues, Magn. Reson. Med. 32 (1994) 592–601.
[4] Q. Ni, J.D. King, X. Wang, The characterization of human compact bone structure changes by low-field nuclear magnetic resonance, Meas. Sci. Technol. 15 (2004) 58–66.
[5] M.A. Schmidt, G.Z. Yang, P.D. Gatehouse, D.N. Firmin, FID-based lung MRI at 0.5 T: theoretical considerations and practical implications, Magn. Reson. Med. 39 (4) (1998) 666–672.
[6] Y. Wu, J.L. Ackerman, D.A. Chesler, J. Wang, M.J. Glimcher, In vivo solid state ^{31}P MRI of human tibia at 1.5 T, in: Proceedings of the 7th Annual Meeting of ISMRM, Philadelphia, PA, USA, Abstract 313, 1999.
[7] Y. Wu, D.A. Chesler, M.J. Glimcher, L. Garrido, J. Wang, H. J. Jiang, J.L. Ackerman, Multinuclear solid-state three-dimansional MRI of bone and synthetic calcium phosphates, in: Proc. Natl. Acad. Sci., vol. 96, No. 4, USA, 1999, pp. 1574–1578.
[8] R. Reddy, E.K. Insko, E.A. Noyszewski, R. Dandora, J.B. Keenland, J.S. Leigh, Sodium MRI of human articular cartilage in vivo, Magn. Reson. Med. 39 (5) (1998) 697–701.
[9] S. Kirsch, M. Augath, D. Seiffge, L. Schilling, L.R. Schad, In vivo chlorine-35, sodium-23 and proton magnetic resonance imaging of the rat brain, NMR Biomed. 23 (2010) 592–600.
[10] X.H. Zhu, N. Zhang, Y. Zhang, X. Zhang, K. Ugurbil, W. Chen, In vivo ^{17}O NMR approaches for brain study at high field, NMR Biomed. 18 (2) (2005) 83–103.
[11] M.D. Robson, P.D. Gatehouse, M. Bydder, G.M. Bydder, Magnetic resonance. An introduction to ultrashort TE (UTE) imaging, J. Comput. Assist. Tomogr. 27 (2003) 825–846.
[12] W. Kuhn, P. Barth, S. Hafner, Material properties of cross-linked polymers by NMR, Macromolecules 27 (1994) 5773–5779.
[13] S.D. Beyea, B.J. Balcom, P.J. Prado, A.R. Cross, C.B. Kennedy, R.L. Armstrong, T.W. Bremner, Relaxation time mapping of short T_2^* nuclei with single-point imaging (SPI) methods, J. Magn. Reson. 135 (1998) 156–164.
[14] J. Du, A. Takahashi, M. Carl, M. Bydder, N. Szeverenyi, C. Chung, G. Bydder, T_2 and $T_1\rho$ quantification of cortical bone in vivo using ultrashort TE (UTE) pulse sequences, Proc. Int. Soc. Magn. Reson. Med. 18 (2010) 3199.
[15] B. Kingsley, Product operators, coherence pathways, and phase cycling. Part III: phase cycling, Concepts Magn. Reson. 7 (3) (1995) 167–192.
[16] N. Bloembergen, R.V. Pound, Radiation damping in magnetic resonance experiments, Phys. Rev. 95 (1) (1954) 8–12.
[17] M.P. Augustine, Transient properties of radiation damping, Progr. Nucl. Magn. Reson. Spectrosc. 40 (2002) 111–150.